PCCP

Accepted Manuscript

Journal Name

ARTICLE TYPE

An integrated superhydrophobic-plasmonic biosensor for mid-infrared protein detection at the femtomole level

Adele De Ninno[a], Gabriele Ciasca*[b], Annamaria Gerardino[a], Eugenio Calandrini[c], Massimiliano Papi[b], Marco De Spirito[b], Alessandro Nucara[3], Michele Ortolani[a,c], Luca Businaro[a] and Leonetta Baldassarre[d]

In this work we present an integrated biosensor that enables FTIR (Fourier Transform – Infrared) spectroscopy of analytes contained in diluted solutions. The fabricated nanosensor allows for the detection of proteins through the identification of their Amide I and II bands fine structure, up to the nanomolar concentration range. We exploited two distinct effects to enhance the sensitivity: i) the concentration effect due to the presence of the superhydrophobic surface that conveys molecules dispersed in solution directly inside the focus of a FTIR spectromicroscope; ii) the plasmonic resonance of the nanoantenna array that provides electromagnetic field enhancement in the Amide I and II spectral region (1500-1700 cm^{-1}). We demonstrate detection of ferritin in the nanomolar concentration range, a blood protein that is usually available in small amounts in typical blood samples.

Introduction

Over the last decade a large effort has been devoted to the development of optical biosensors enabling the detection of analytes in highly diluted solutions. Among the sensors being developed, those offering a precise detection of blood proteins at molar concentration precision in the 10^{-9} mol/l range are indeed emerging as a fundamental prerequisite for the early diagnosis of relevant pathologies including Alzheimer disease and several types of cancer. Several classes of ultrasensitive devices have been proposed, such as fluorescence-based biosensors [1], refractive index biosensors [2-4], Raman spectroscopy and infrared biosensors operating both in the near (NIR) and mid-infrared (MIR) range [5-8]. Among these devices, those operating in the MIR range are very promising since they directly target specific biomolecular classes like proteins or lipids and, in the case of proteins, they allow gathering information about the secondary structures content and conformational changes through the spectroscopic determination of the fine structure of the protein Amide I and II bands centered, respectively, at 1660 cm^{-1} and 1537 cm^{-1} [9].

However two fundamental shortcomings hinder the MIR biosensor performances. First, at low protein concentrations, devices sensibility is usually limited by the efficiency of analyte delivery to the sensing surface that often exploits passive transport pathways, thus hampering the fabrication of high throughput and cost effective devices. Second, MIR spectroscopy, being a linear absorption technique, is plagued by a strong thermal emission background that makes the signal-to-noise ratio of few-molecule thick samples very small if compared e.g. to the fluorescent-label based methods, that are virtually background-free.

To overcome these two limitations many strategies have been adopted.

The analyte transport problem has been recently addressed by De Angelis and co-workers [10]. They employed superhydrophobic microstructured surfaces to drive and concentrate molecules over the sensing area of a Raman microspectroscopy nanosensor. The same analyte concentration technique based on superhydrophobic surfaces was then used for X-ray diffraction and X-ray fluorescence measurements, mass spectroscopy measurements and for the precise positioning of DNA strands [11-17].

The development of plasmonic nanostructures able to provide local electromagnetic field enhancement in nanometer-scale hotspots has recently emerged as an effective method to improve the signal-to-background ratio of MIR biosensors, enabling the detection of very low amounts of proteins down to zeptomoles [6]. Therein, the key feature was a careful design of plasmonic dipole nanoantenna arrays, with resonance frequency finely tuned at the protein Amide I band [6,7,9].

In this work we fabricate and test an integrated MIR biosensor for protein detection from diluted pure protein solutions. A sensitivity down to the nanomolar concentration range is obtained by combining the strong field enhancement provided by plasmonic nanoantenna arrays with the superhydrophobic patterned surface: the molecules present in a 5 µl solution droplet are directly conveyed on the sensing part of the device where the MIR optical beam is focused. Protein detection in a label-free and non-destructive fashion is demonstrated. Moreover, the achieved device sensitivity enabled the measurement of the secondary structures of the protein ferritin. This latter feature of our biosensor opens the way for the detection of subtle conformational changes of blood proteins that are often found at

low concentrations in typically available blood samples. Therefore, the device here discussed, combined with already available biochemical purification methods, can find its own field of application in the study of clinically relevant proteins, such as blood ferritin that has been very recently proposed as a relevant parameter for the early detection of Alzheimer Disease [18-21].

Material and methods

Device fabrication

The integrated mid-IR plasmonic device was fabricated by a two-step lithographic process. In the first one the fabrication of rod-shaped gold nanoantenna arrays with plasmonic resonances tuned at the Amide I and/or Amide II bands is performed. The second step consisted of the fabrication of superhydrophobic frame, encircling the nanoantenna array, aimed at concentrating highly diluted samples directly on the array.

All the fabrication steps were carried out using a VISTEC EBPG-5HR, equipped with a field emission gun operated at 100 kV, allowing a resolution down to the 20 nm linewidth.

In details, for each device a 400 x 400 μm^2 plasmonic gold nanoantenna array was first fabricated directly on a silicon substrate. A 450 nm-thick ZEP-520A resist layer was spun on substrate surface, e-beam exposed and developed in oxylene to define a pattern including the nanoantenna array and a set of alignment markers.

 A 30nm Chromium adhesion layer followed by a 140 nm-thick gold layer was then deposited by e-gun assisted evaporation. After lift-off in anisole, perfectly defined Cr/Au nanorod structures were formed. Fig. 1A shows a SEM image of one of the fabricated arrays, consisting of 1250 nm long, 210 nm wide and 150 nm thick nanorods, with a periodicity of 1650 nm.

A gold frame surrounding the nanoantenna array was also included in the pattern to avoid MIR radiation spillover outside the array(Fig 1B). Then, a 1.2 μm thick layer of PMMA-950K-9% positive tone resist was spun on the substrate and patterned using e-beam lithography after re-alignment on the markers.

 A 2D array of squares (5 μm side; 9 μm distance) and a square-shaped central region (side: 500 μm) containing the nanoantenna array is then transferred on the substrate by means of a Inductively Coupled Plasma-assisted dry etching of the Silicon substrate, using PMMA as masking layer. The final etch depth was 22 μm, which created a field of square micropillars, encircling the central nanoantenna region, with aspect ratio higher than 4, and distance smaller than the pillar height. This microstructure, shown in Fig. 1C, is the prerequisite for the superhydrophobic behavior as explained below.

After cleaning in piranha solution ($H_2SO_4:H_2O_2$=3:1), the device surface was silanized to impart the superhydrophobic behavior with 10% trimethylchlorosilane (TMCS, $(CH_3)_3SiCl$, FluKa, purchased by Sigma Aldrich (CAS number 75-77-4)) in toluene, kept in a nitrogen environment for 48 h, followed by a rinse in methanol and n-heptane.

The device was then spin coated with a layer of S1813 positive photoresist and the central region containing the nanoantennas was exposed to a i-line (365 nm) UV light source through an aligned photomask, and the resist was developed. The

hydrophobic coating was then removed from the central region only by means of a Reactive Ion Etching process, which etches a few tens of nanometers of silicon from the silanized surface.
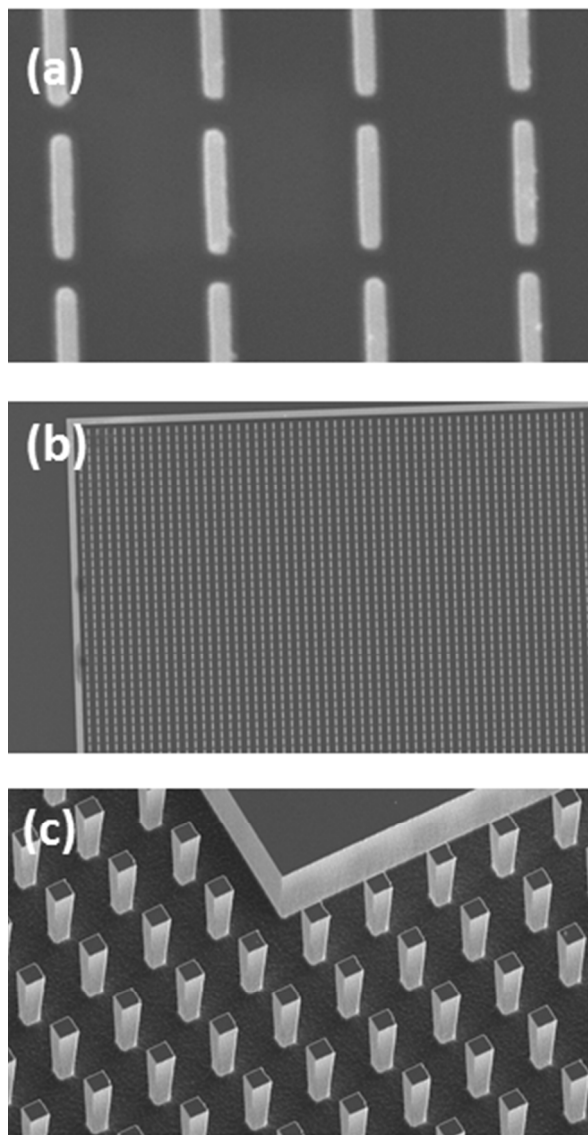

Fig.1 Panel a-b: SEM micrographs of the fabricated periodic nanoantennas array, consisting of 1250 nm long, 210 nm wide and 150 nm high rods with a periodicity of 1650 nm. Panel c: SEM micrograph of the superhydrophobic patterned surface.

IR measurements

The transmittance and reflectance of the plasmonic nanostructures were measured by means of a reflective-objective microscope coupled to a FTIR spectrometer (Bruker IFS 66v/S). For both measurements, square apertures of 100 μm side were used to illuminate with the IR beam only the internal part of the nanoantenna array, whose size of 400x400 μm^2 was then in large excess of the illuminated area, so as to safely exclude radiation spillover. The reflectance was calculated through the ratio $R = I_{sample}^R/I_{gold}^R$, where I_{sample}^R is the intensity of radiation reflected by the sample and I_{gold}^R is the intensity reflected by a

150-nm-thick Au film evaporated on the same substrate. The transmittance was instead measured against a double-side polished Si wafer.

Linear-polarization dependent measurements were acquired by using a KRS-5 wire-grid polarizer (by Specac). Only reflectance measurements will be discussed, as the transmitted intensity was heavily suppressed by the back face roughness. This problem will be targeted in the next generation of devices.

Results and discussion

Active mass transport by means of superhydrophobic surfaces

An electron microscope image of the integrated plasmonic biosensor is shown in fig. 2a. Three different regions formed by three concentric squares of decreasing size can be clearly distinguished: i) a superhydrophobic region of 2.5x2.5 mm^2 consisting of an array of square silicon pillars (height: 22 μm, width: 5 μm, pitch: 14 μm, empty space between pillars: 9 μm) ii) a hydrophilic region of 500x 500 μm^2 which serves as anchorage point for a solution droplet that is cast on the device; iii) a plasmonic nanoantenna array of 400x 400 μm^2, that provides electromagnetic field enhancement in the spectral region of the Amide I and II bands. Fig. 2b to 2e show the behavior of a 5 μl droplet deposited on our device: the anchorage region binds the drop, allowing its deposition in a well-defined position (fig 2b).

At this stage, the drop assumes a contact angle of 146°±5° (more details can be found in SI section). During evaporation, the drop reduces in volume while maintaining its quasi-spherical shape. This is made possible by the peculiar geometry of the patterned surface.

The superhydrophobic region is indeed specifically designed to be wetted in the Cassie-Baxter state.

This suspended configuration allows the evaporating drop edge to slide above pillars maintaining its initial shape. Under evaporation, the solution becomes more and more concentrated maintaining, at the same time, a good on-target confinement (fig 2c and 2d). Further details on the droplet dynamic under evaporating conditions can be found in refs [22,23]. At the end of the process, the drop collapses (fig 2e) depositing the solute within the hydrophilic region containing the sensing plasmonic surface. The concentration effect provided by this method allows to actively convey few molecules directly on the sensing area where the MIR optical beam is focused (see the sketches in Fig 4a and 4b).

Detection of ferritin at the femtomole level

In Fig. 3 the reflectance spectrum of one of the fabricated nanoantenna arrays is shown. The effect of the polarization direction of the electric field vector of the incident radiation is apparent in Fig. 3a. For electric field polarized parallel to the long axis of the rod shaped antennas (E$_{//}$), a broad reflectance peak centered at 1660 cm^{-1} and about 400 cm^{-1} wide at half peak height can be clearly observed.
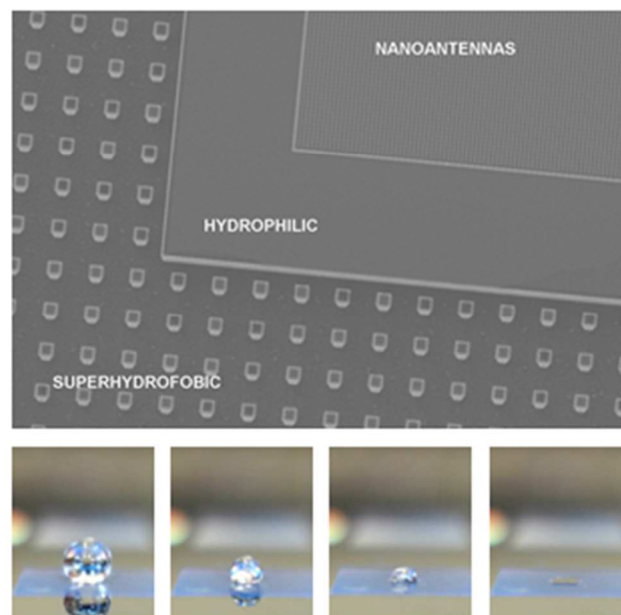

Fig. 2 Panel a: SEM micrograph of the fabricated device. The periodic array of pillars – that induces the superhydrophobic behavior - and the square shaped hydrophilic pad containing the nanoantennas can be clearly recognized. Panel b-e: behavior of 5 microliter droplet deposited on our device under controlled evaporation conditions.

Conversely, for electric field polarized perpendicular to the rod-shaped antennas , the plasmonic resonance is not excited in the spectral range of interest. The peak in the E$_{//}$ reflectance spectrum of Fig. 3a is due to the resonant plasmonic excitation of the nanoantennas and it is an indication of field enhancement by a factor around 100 in a region of few tens of nanometers at the gold surface [6,7].

A resonance Q factor (Q=ν$_0$/Δν) of 3.9±0.2 has been calculated by means of a Lorentzian fit. The resonance peak shown in Fig. 3A is centered at 1600 cm^{-1}, exactly in between the protein Amide I and Amide II vibrational absorption bands. To obtain this fine spectral tuning, several nanoantenna arrays have been realized by varying both the periodicity of the array and the length of the gold nanorod. As expected, when all the design dimensions were rescaled proportionally to a factor C, we verified a linear scaling with C of the resonance peak frequency in the range 1550-2000 cm^{-1}[9].

Taking advantage of the strong field enhancement at the gold surface which produces the resonance peak of Fig. 3a [6,7], we investigated the capability of our device to detect small amounts of proteins.
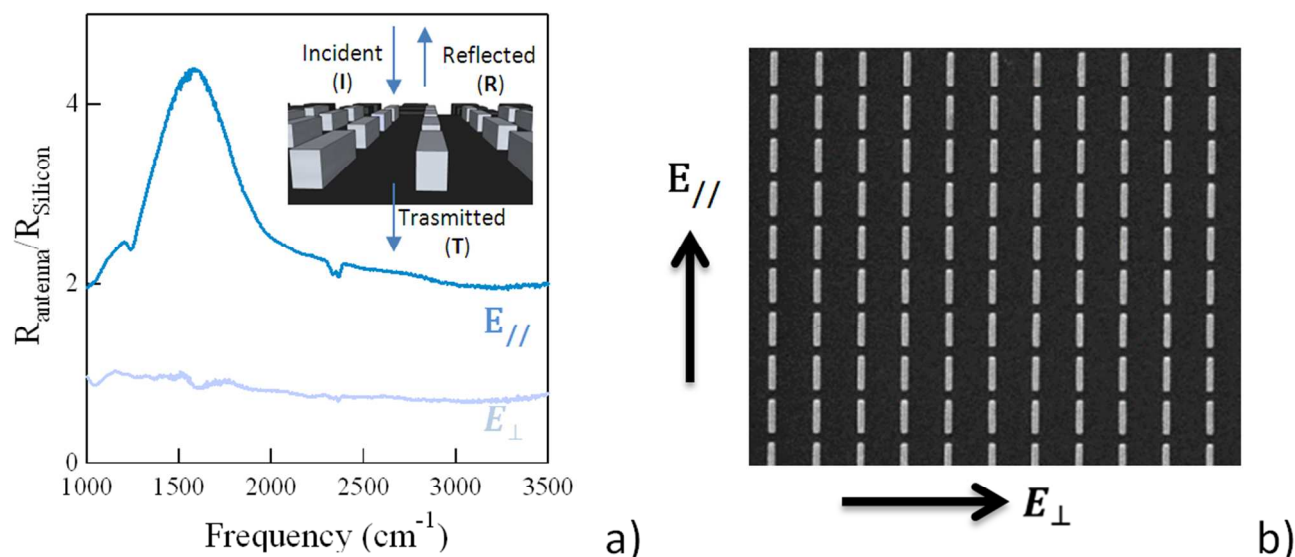
ARTICLE TYPE

Fig.3 Panel a: Reflectance spectra of the nanoantennas array for two different polarization, parallel ($E_{//}$) and orthogonal ($E_\perp$) to the long axis of the rod shaped antennas. Panel b: SEM micrograph of the measured nanoantennas array that highlights the electromagnetic field direction.

A schematic view of the measurement geometry is shown in fig 4a and 4b.

FTIR measurements are acquired by using an infrared microscope at normal incidence collecting the reflected light (see methods). Apoferritin is a globular protein composed of 24 subunits assembled in a large spherical complex, which has been used for testing the present device. Given its well-defined, robust and dominantly α-helical secondary structure content, apoferritin was ideally suited for this purpose.

Each apoferritin subunit is indeed composed of six α-helix and only one β-turn , so it should provide an Amide I vibrational absorption line shape predominantly centered at 1650 cm^{-1} (while a fully β-sheet structure would give an Amide I peak centered at 1625 cm^{-1}[21]).

We prepared a 2 nM apoferritin solution dissolved in 0.1X PBS (Phosphate Buffer Solution containing 0.8g of NaCl, 0.02g of KCl, 0.26g of Na_2HPO_4 0.027g of KH_2PO_4) and we deposited a 5 μl droplet on the device. To distinguish whether spectral signatures comes from the buffer or from proteins, a 5 μl PBS-only drop was also deposited on an identical device.

The protein solution drop contains about 10 femtomoles of proteins. According to the discussion reported above, such amount of protein is actively conveyed directly on the sensing surface of the device thanks to the controlled evaporation dynamic imposed by the superhydrophobic surface.

Assuming an homogeneous distribution of molecules on the hydrophilic pad, we estimate the deposition of a 200 nm-thick layer of apoferritin adsorbed on the sensing part of the device. In fig. 4c three reflectance spectra are displayed: i) the reflectance of the bare nanoantenna array showing the plasmonic resonance (blue continuous line); ii) the reflectance spectrum of the PBS buffer after complete solvent evaporation (cyan continuous line); ii) the reflectance spectra of the protein solution, again, after complete solvent evaporation (violet continuous line). All spectra have been acquired by using an electric field polarization direction along the axis of the rod-shaped antennas ($E_{//}$). A dip absorption peak at 1658 cm^{-1} can be clearly observed in the third curve. This spectral signature is absent in the other curves and, therefore, it can be ascribed to the deposited Apoferritin layer. The signal response to a variety of ferritin amounts in the range 10-100 femtomoles has been reported in the supplementary information (Fig S3, SI section).

In Fig. 5 the corresponding absorption spectrum is reported. This was computed by assuming a double-transmission geometry through the protein layer through the relation $A = -log_{10}(R_{sample}/R_{silicon})$ derived from the Lambert-Beer's law. Due to both the strong assumptions and the inhomogeneous radiation electric field distribution, the absorbance is only proportional to the absorption coefficient, and no quantitative information can be retrieved from Fig. 5.

Clear spectral signatures can be observed in the Amide I and II spectral region.

A feature of note is the presence of a pronounced maximum in the absorption intensity centered at 1655 cm^{-1}. This maximum can be assigned to the vibrational modes of α-helical structures, in agreement with the expected secondary structures content of apoferritin. Measures performed on identical devices show excellent repeatability.

It is worth stressing that the signal-to-background absorption ratio achieved in our device due to the combined use of plasmonics and superhydrophobicity allows to clearly identify the spectral

signatures of 10 femtomoles of protein even without subtraction of the background reflectance.

We estimate the presence of $6 \cdot 10^9$ molecules in our 10 femtomoles sample (4.5 ng of protein) that corresponds to about $2.6 \cdot 10^{13}$ peptide bonds. These numbers are large if compared to those reported in ref [6], where a plasmonic sensor similar to that here presented is described. In this paper authors estimate that absorption arises form an amount of $1 \cdot 10^{-3}$ ng of silk fibroin i.e. about 300 zeptomoles. However, device sensitivity is calculated by considering only the detection volume at the close vicinity of the nonorod tips. A similar calculation can be performed for our device. In our case absorption arises from a 100 μm x 100 μm area in the focal plane defined by the microscope aperture, similar to the case of the above mentioned paper. The physical gold structure of the nanoantennas covers about 30% of this area and we shall take this value as a measure of the sensor cross-section, although the filling fraction of the plasmonic hotspots is even smaller. Taking into account that ferritin forms a 200 nm-thick film, we end up in an effective interaction volume of $1.8 \cdot 10^{11}$ nm3. This volume contains about $8 \cdot 10^7$ ferritin molecules i.e. ~0.14 femtomoles and ~$3.3 \cdot 10^{11}$ peptide bonds.

These values are comparable to those reported in ref [6]; even slightly lower as far as moles are concerned. However this difference is likely to be ascribed to the higher molecular weight of ferritin with the respect to the silk protein, rather than to a higher device sensitivity.
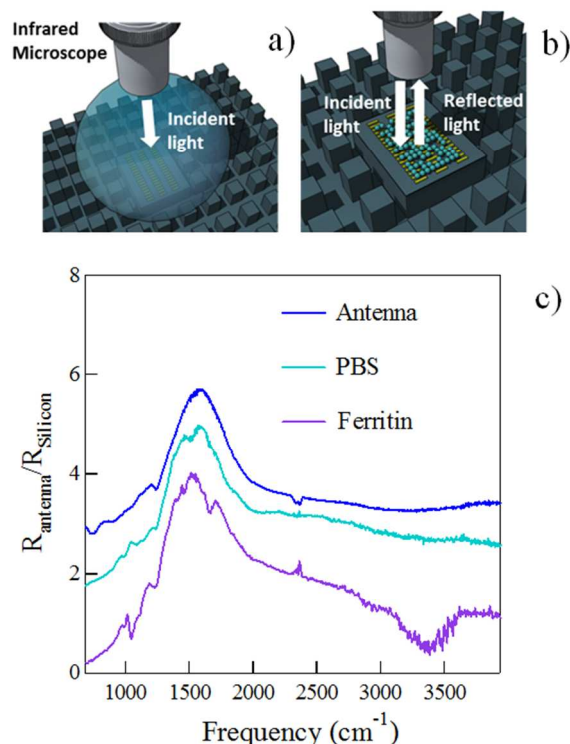

Fig.4 Panel a-b: Schematic view of the measurements geometry. An infrared microscope is used to focus the incident light directly on the hydrophilic pad containing the nanoantennas. After drop evaporation, reflected light is collected. Panel c: Reflectance spectra of the bare nanoantenna array (blue continuous line), the buffer solution without proteins (cyan continuous line) and a solution containing apoferritin (initial concentration 0.001 mg/ml). All spectra have been acquired in dry

environment by using electric field polarization direction parallel to the nanoantenna axis.

Although our device allows protein detection through the identification of specific vibrational modes with a sensitivity down to about 10 femtomoles, nevertheless higher amounts are required to perform a detailed spectral analysis of the Amide I band. This task can be achieved by measuring 100 femtomoles of proteins dissolved in a 5 μl drop, which corresponds to an initial protein concentration of 0.01mg/ml. In the SI section we analyze the Amide I absorption band by Gaussian curve-fitting together with second derivative methods [24-27]. The recovered secondary structures are consistent to those expected for a ferritin sample under folding conditions. The present results clearly point out that our integrated nanosensor can be used for protein detection and secondary structures identification down to the femtomole range. However a more in-depth study is required to assess the extent of the secondary structures modifications that may occur during the evaporation process in case of protein that are particularly sensitive to hydration shell. Therefore a particular care must be taken when using our device to measure this class of proteins.
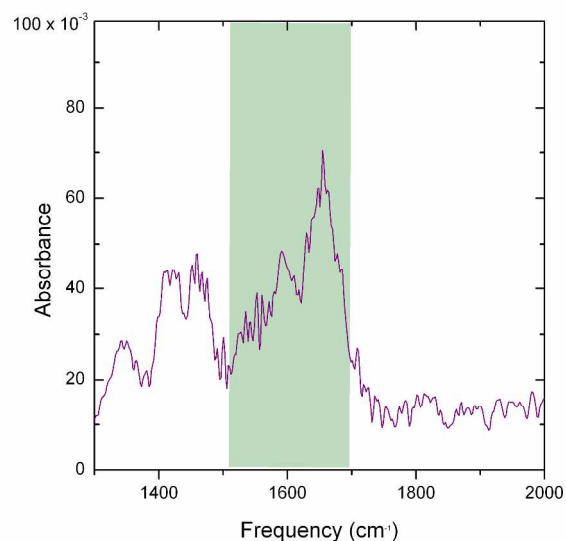

Fig.5 Measured Absorbance spectrum in the Amide I and II spectral region of the Apoferritin solution after drying. The units of the left axis are arbitrary. The color-shaded region highlights the Amide I and II range.

Conclusions

In this paper we fabricate and test an integrated biosensor capable to provide good-quality FTIR absorbance spectra down to the femtomole range. The fluidic transport is obtained by engineering superhydrophobic surfaces, overcoming the inherent limitations of passive transport. Our device has the potential to measure the secondary structures content of proteins under study, a feature not available, for example, in refractive-index plasmonic sensors operating in the UV-VIS range that probe mass accumulation in the presence of a substance-specific capture layer but cannot provide structural information on the measured samples.

A major improvement in the sensitivity of the FTIR technique to small concentration levels of proteins in solution below the micromolar range is offered by the joint use of plasmonic

nanostructures designed to have electric field enhancement in the Amide I and II spectral range, i.e. 1500-1700 cm^{-1} .

Apoferritin, a spherical protein complex that has its main function in cellular iron storage, has been used for testing the device for its high content of stable α-helical structures. Our device was successfully used to both demonstrate the detection of about 10 femtomoles of protein and clearly distinguish spectral signatures of the apoferritin α-helical structures. Plasma ferritin concentration in blood can indeed vary from less than 10 μg/L to 1–10 mg/L in response to various clinical conditions. A single blood sampling contains a ferritin amount ranging between few tents of femtomoles to few picomoles. Therefore the achieved device sensitivity allows the detection of ferritin and the determination of its secondary structure content directly from a single blood sampling. This is particularly important since elusive conformational modifications of plasma ferritin have been proposed as a relevant parameter for the early detection of Alzheimer Disease. Therefore, the proposed technology may boost the development of novel diagnostic tools able to detect subtle conformational changes in blood proteins that provide high value clinical information but are available in small amounts in typical blood samples. However, it is worth stressing here that the described device, as well as similar devices based on MIR spectroscopy, requires the use of purified protein solutions and therefore must be used in combination with existing biochemical purifications methods. This is especially true in the mention case of serum ferritin, since blood contains a large number of more abundant protein molecules with similar secondary structure content, such as albumin.

Notes and references

^{a} CNR-Istituto di Fotonica e Nanotecnologie, Via Cineto Romano 42, 00146 Rome, Italy

^{b} Istituto di Fisica, Università Cattolica del Sacro Cuore, Largo F. Vito 1, 00168 Rome, Italy E-mail: gabriele.ciasca@rm.unicatt.it

^{c} Dipartimento di Fisica, Università di Roma "La Sapienza", Piazzale Aldo Moro 5, I-00185 Rome, Italy

^{d} Center for Life Nano Science, Istituto Italiano di Tecnologia, Viale Regina Elena 291, 00161 Rome, Italy

1   S. Wang, S. Ota, B. Guo, J. Ryu, C. Rhodes, Y., Xiong, , ... and X. Zhang, *Nano letters*, 2011, **11**(8), 3431-3434.
2   S. Aksu, A. Yanik, R. Adato, A. Artar, M. Huang, and H. Altug, *Nano letters*, 2010, **10**(7), 2511-2518.
3   N. Ramachandran, D. Larson, P. Stark, E. Hainsworth and J. LaBaer *Febs Journal,* 2005, **272**, 5412-5425.
4   E. Özkumur, J.W. Needham, D.A. Bergstein, R. Gonzalez, M. Cabodi, J.M, Gershoni,... and M.S. Ünlü, *Proceedings of the National Academy of Sciences*, 2008, **105**(23), 7988-7992.
5   M. Golosovsky, V. Lirtsman, V. Yashunsky, D. Davidov and B. Aroeti, *Journal of Applied Physics*, 2009, **105**(10), 102036-102036.
6   R. Adato, A.A. Yanik, J.J. Amsden, D. L., Kaplan, F. G. Omenetto, M.K. Hong,... and H. Altug, *Proceedings of the National Academy of Sciences*, 2009, **106**(46), 19227-19232.
7   R. Adato and H. Altug, *Nature communications*, 2013, **4**.
8   J. M. Rui Tan, J. J. Ruan, H. K. Lee, I. Y. Phang, and X. Yi Ling, Phys. Chem. Chem. Phys., 2014,**16**, 26983-26990.
9   L. Businaro, O. Limaj, V. Giliberti, M. Ortolani, A. Di Gaspare, G. Grenci,... and S. Lupi, Microelectronic Engineering, 2012, 97, 197-200.
10 F. De Angelis, F. Gentile, F. Mecarini, G. Das, M. Moretti, P. Candeloro, ..and E. Di Fabrizio, *Nature Photonics*, 2011, **5**(11), 682-687.
11 A. Ressine, G. Marko-Varga, and T. Laurell, *Biotechnology Annual Review*, 2007, **13**, 149-200.
12 G. Ciasca, L. Businaro, M. Papi, A. Notargiacomo, M. Chiarpotto, A. De Ninno,... & M. De Spirito, *Nanotechnology*, 2013, **24**(49), 495302.
13 G.Ciasca, M. Papi, M. Chiarpotto, A. De Ninno, E. Giovine, G. Campi, A., Gerardino, M. De Spirito and L. Businaro, *Nano-Micro Letter*, 2014, **6**(3), 280-286.
14 A.Accardo, M. Burghammer, E.D. Cola, M. Reynolds, E.D. Fabrizio, and C. Riekel, *Langmuir*, 2011, **27**(13), 8216-8222.
15 G. Ciasca, M. Papi, V. Palmieri, M. Chiarpotto, S. Di Claudio, A. De Ninno, E. Giovine, G. Campi, A. Gerardino, L. Businaro, M. De Spirito, acceted for pubblication on *Nano-Micro Letter* DOI 10.1007/s40820-014-0027-z
16 L. Businaro, O. Limaj, V. Giliberti, M. Ortolani, A. Di Gaspare, G. Grenci,... and S. Lupi, Microelectronic Engineering, 2012, **97**, 197-200.
17 G. Ciasca, L. Businaro, A. De Ninno, A. Cedola, A. Notargiacomo, G. Campi,... and A. Gerardino, *Microelectronic Engineering*, 2013, **111**, 304–309.
18 P. De Sole, C. Rossi, M. Chiarpotto, G. Ciasca, B. Bocca, A. Alimonti,... and C. Masullo, Clinical biochemistry, 2013, **46**(1), 89-93.
19 M. Chiarpotto, G.Ciasca, M. Vassalli, C. Rossi, G. Campi, A. Ricci, andM Papi, Applied Physics Letters, **103**(8), 083701.
20 J.Bester, A.V. Buys, B. Lipinski, D.B. Kell, and E. Pretorius, Frontiers in aging neuroscience, 2013, **5**.
21 G. Ciasca, M. Papi, M. Chiarpotto, M. Rodio, G. Campi, C. Rossi, P. De Sole, and A. Bianconi APPLIED PHYSICS LETTERS 100, 073703 (2012)
22 S. Dash, A. Chandramohan, J. A. Weibel, and Sures V. Garimella, PHYSICAL REVIEW E, 2014, **90**, art no. 062407
23 M. Dicuangco, S. Dash, J. A. Weibel1 and S. V. Garimella , Appl. Phys. Lett., 2014, 104, art no. 201604
24 A.Nucara, P. Maselli, V. Giliberti and M. Carbonaro, *SpringerPlus, 2013, 2*, 661.
25 E. Goormaghtigh, V. Cabiaux, J. M. Ruysschaert, FEBS, 1990. 193, 2, 409-420.
26 M. Jackson and H. H. Mantsch, Critical Reviews in Biochemistry and Molecular Biology, 1995, 30(2):95-120.
27 D. Michael Byler andHeino Susi, Biopolymers, 1986, **25**(3):469-487
28 I. Listowsky , G. Blauer , S. Englard , J. J. Betheil Biochemistry, 1972, **11** (11), pp 2176–2182